Materials Research Express 4(6) (2017) 065501

Zr-doped TiO_2 nanoparticles synthesized via a sol-gel route and their application in dye-sensitized solar cells for thermo-stabilization

Anastasia Pasche[1], Bernd Grohe[1], Silvia Mittler[1,2], Paul A. Charpentier[1]*

[1]Department of Chemical and Biochemical Engineering, The University of Western Ontario, London, Ontario, N6A 5B9, Canada

[2]Department of Physics and Astronomy, The University of Western Ontario, London, Ontario, N6A 3K7, Canada

Abstract

Dye-sensitized solar cells (DSSCs) are regarded as one of the most promising solar cells amongst third-generation photovoltaic technologies, particularly due to their low cost, easy preparation, and minor environmental impact compared to earlier-generation devices. However, they have been challenged by thermal energy losses and low cell efficiencies. This work examined the incorporation of zirconium (Zr) into the crystal lattice of titania nanoparticles ($nTiO_2$) for subsequent fabrication into the photo anode of the DSSCs. The results showed that Zr doping of $nTiO_2$ inhibited the anatase-rutile phase transition. Higher calcination temperatures gave increased titania crystallinity, and stabilized the $nTiO_2$ aggregate pore structure and specific surface area, consequently improving the DSSC device performance. A doping concentration of 5 mol % Zr into the $nTiO_2$ demonstrated the best resistance against thermal degradation, achieving an optimized retention of specific surface area. Solar simulation confirmed the results, indicating better heat stability, although lowering the DSSC efficiencies.

Key words: TiO_2 nanoparticles; Zr doping; thermostabilization; DSSC; photoanode

1. Introduction

When a dye-sensitized solar cell's (DSSC) photoactive material is illuminated, the energy taken up from the incident light is partly absorbed. The dissipation of energy due to absorption may give rise to several secondary effects, including local heat production. One of the assumptions of the Shockley-Queisser limit [1] is that excited electrons created by high-energy photons are immediately relaxed to the bandgap edge: the energy fraction of photons with energies larger than the bandgap is immediately lost as heat, a phenomenon referred to as thermalization. Thus, a temperature increase in operating solar cells is always present.

Active layers in DSSCs consisting of nano-porous TiO_2 are only some tens of micrometres thick, enabling flexible applications. However, flexible plastic substrates, which are typically used, cannot tolerate process temperatures of up to 500°C, common for the calcination of TiO_2 nanoparticles. There have been investigations into the development of hybrid nanowire/nanoparticle structures through low temperature (<90 °C) processes that provide the dual advantages of the nanoparticles' large surface area for dye adsorption and the nanowires' efficient electron transport [2]. However, device demonstrations have been limited due to the inability of the nanoparticles to adequately permeate the densely-packed forest of nanowires.

It is important to be able to maintain a stable mesoporous thin film structure since it determines the specific surface area and charge carrier transport path of the material. Some approaches have shown that it is possible to control the mesophase-ordering and macroscopic morphology using structure-directing agents and optimizing annealing temperature and time [3,4]. A small amount of transition metal doping has also been found

to very effectively improve the thermal stability and activity of titania (TiO_2) [5-11]. Zirconium (Zr), for instance, is one of these suitable dopants, as it is known to have very high thermo-stabilizing properties [12,13]. It's oxide, zirconia (ZrO_2), which can be formed while doping TiO_2 with Zr, is transparent and has one of the highest dielectric constants known for metallic oxides [14]. Therefore, it exhibits interesting optical properties as well. Additionally, ZrO_2 is chemically very stable due to its multi-electronic configuration, including the Zr's d-orbital electrons, a characteristic for transition metals. There are several explanations provided for zirconium's thermo-stabilizing effects on the TiO_2 crystal lattice of anatase. First, Ti and Zr are located in the same group of elements (IVB) giving them comparable physicochemical properties. However, Zr^{4+} ions are larger in size and more electropositive than Ti^{4+}. Thus, Zr^{4+} ions are more inclined to accept the electrons of O^{2-}. As a result, the neighbouring Ti-O bonds in the lattice become more stable and more difficult to break, increasing the lattice's stability at elevated temperatures [15,16]. It is, therefore, ZrO_2, which provides the thermo-stabilizing effect. The thermo-stabilizing properties can also be attributed to ZrO_2's relatively large band gap (~5eV), making it more electrically insulating than TiO_2. These factors could prove useful in decreasing the heat produced during cell operation.

Miao et al. [17] have reported on the attractive thermal stability of mesoporous Zr-oxophosphate as a solid acid catalyst, because its ordered structure could be maintained even when treated at 800º C. Similarly, Lucky et al. [12] have found that the presence of ZrO_2 in a matrix of TiO_2 nanotubes helped to preserve the nanostructure during high-temperature heat treatment. There is plenty of evidence that ZrO_2 in the TiO_2 crystal lattice

increases thermal stability and preserves structures of the photoactive material in DSSCs at high temperatures [12,13,17,18].

For sol-gel synthesized $nTiO_2$ powders, Kim et al. [19] found a bimodal porosity which consists of large intra-NP pores in the order of ~50-100 nm (due to voids between NPs making up the aggregates) and small pores of 2-5 nm within the NPs (the NPs are composed of crystallites). Zr-doping allowed maintaining pore populations up to relatively high calcination temperatures. However, an extensive analysis on the optimal doping concentration, in particular for DSSCs, is still missing.

Although incorporating Zr^{4+} into the TiO_2 crystal inevitably introduced lattice defects, the presence of a few defects can improve the photo-electrochemical activity of a photoactive $Zr_xTi_{1-x}O_2$ layer-based DSSC device. However, an excess of defects will promote charge recombination and a decrease of the DSSC efficiency. Therefore, a low Zr-doping concentration can be beneficial by reducing the TiO_2-bandgap due to establishing states just below the conduction band (CB). Moreover, a reduced photon energy threshold is required to excite electrons into the CB. However, increasing the Zr-concentration also plays a role in creating charge-trapping centers [20], typically grain boundaries that have a negative effect on electron conduction. Additionally, the literature discusses how Zr concentrations beyond 50 mol % can cause an increase of the bandgap attributed to quantum-size effects [21]. Increasing the already large bandgap of TiO_2 would be unfavorable for low-energy photon harvesting. Therefore, the doping concentrations investigated here did not exceed 15 mol %.

In the present study, Zr-doping concentrations between 0 and 15 mole % in $nTiO_2$ photoactive materials were established to determine the optimum concentration for thermo-

stabilization in DSSCs. These Zr-doped photoactive materials ($Zr/nTiO_2$) were integrated into DSSCs to achieve improved photovoltaic efficiency via thermo-stabilization with Zr. The structural and compositional properties of the prepared binary oxides were investigated using x-ray diffraction (XRD), surface area analysis, and electron microscopy. Solar simulation was used to determine the energy conversion efficiencies of the $Zr/nTiO_2$ composites in DSSCs. Zirconium's thermo-stabilizing effect offers the possibility for new solar cell designs with smaller semiconductor thicknesses and thus lower material and device fabrication costs. Amortization of investment for an alternative energy generation will be substantially shorter. This has crucial technical and strategic consequences, as the photovoltaic industry is predicted to scale-up in manufacturing capacity from its present level of a few GW to over 200 GW by the year 2050, and eventually to the TW-scale very soon.

2. Experimental

A sol-gel route adapted from Chen et al. [22] was used to prepare pure $nTiO_2$ and $Zr/nTiO_2$. Titanium *n*-butoxide (TBO; 97%), zirconium *n*-butoxide (ZBO; 80%) acetylacetone (acac; >99%) and ethanol (EtOH; 99.7%) were all purchased from Sigma Aldrich (Oakville, ON, Canada) and used as received. Hydrochloric acid (HCl; 37%) was purchased from Caledon Labs (Georgetown, On, Canada). For the preparation of $nTiO_2$, a solution of ethanol, HCl and H_2O (for concentrations see Table 1) was added dropwise to a mixture of TBO and acetylacetone in ethanol (for concentrations see Table 1) that was heated to 50º C, and kept under vigorous stirring for 5 h to ensure proper gel formation. Solvent evaporation was accomplished by a rotary evaporator and subsequently dried in a

vacuum oven at 60º C overnight. The dry porous gel was separated into 4 equal allotments and calcined at 400° C, 500° C, 600° C, and 700º C for 4 h with an initial temperature ramp of 10º C/min. The obtained powders were subsequently milled using mortar and pestle. For the preparation of Zr/nTiO_2, the Zr-dopant was admixed to the reaction via co-hydrolysis. This method allows for precise control of the dopant concentration and homogeneous mixing of the precursors. Molar amounts of reactants for nTiO_2 and Zr/nTiO_2 are summarized in Table 1.

Table 1: Experimental conditions used for sol-gel reactions.

Reagent	Amount (mol)			
	0 mol % ZrBu	5 mol % ZrBu	10 mol % ZrBu	15 mol % ZrBu
Ti *n*-butoxide	0.2	0.19	0.18	0.17
Zr *n*-butoxide	-	0.01	0.02	0.03
Acetylacetone	0.2			
EtOH	0.685 (twice)			
HCl	0.01			
H_2O	0.8			

In total, 16 samples were prepared: Zr/nTiO_2 of 0, 5, 10 and 15 mol %. Each sample was calcined at T = 400° C, 500°C, 600° C, and 700 ° C to investigate thermo-stabilization properties of the Zr modification. The Zr concentration in mole % is abbreviated as % in the figures.

The crystal structures of nTiO_2 and Zr/nTiO_2 were analyzed by x-ray powder diffraction (XRD) using a Bruker AXS D2 Phaser diffractometer (Bruker, Billerica, Ma, USA) with Cu Kα radiation. The identification of crystal structures was carried out with the help of the JCPDS cards 00-021-1272 and 79-1771, for tetragonal TiO_2 anatase and

tetragonal ZrO_2 zirconia, respectively. The specific surface area (SSA) of the powders was determined by applying the Brunauer-Emmett-Teller (BET) theory to N_2 adsorption-desorption isotherms obtained from a Micromeritics TriStar II 3020 surface area and porosity instrument (Micromeritics Instrument Corporation, Norcross, GA, USA). The morphology of the samples was investigated by scanning electron microscopy (SEM) using a LEO-Zeiss 1540 XB microscope (Zeiss, Oberkochen, Germany) equipped with an Oxford Instruments x-ray system (Abingdon, UK) allowing for in-situ elemental mapping and analysis (EDS). Finally, the energy conversion efficiency of DSSCs comprising the $Zr/nTiO_2$ samples as the photoactive layer was measured using the simulated illumination of a Newport Oriel 92250A-1000 (Irvine, Ca, USA) solar simulator and a Keithley 2420 digital source meter (Cleveland, Oh, USA). DSSCs were fabricated according to the procedure described in the supporting information (SI). A pure $nTiO_2$ powder (P25) with an average particle size of 21 nm was purchased from Degussa (Degussa P25, Aeroxide, Evonik Canada, Toronto) and used for comparison in some experiments.

3. Results and Discussion

As described in Table 1, 16 different $Zr/nTiO_2$ samples were prepared containing 0, 5, 10 and 15 mol % Zr, each calcined at T = 400° C, 500°C, 600° C, and 700 ° C to investigate the thermo-stabilization properties of Zr modification. The Zr concentration in mole % is abbreviated as % in the figures. First, XRD of the resulting powders was studied, and specific surface areas analyzed by BET to examine, e.g., the porosities of samples. Electron micrographs provided additional information about the powders, such as

particle/cluster sizes. Finally, the DSSC performance was studied by photocurrent density-voltage (J-V) diagrams.

3.1 Effect of Zr Doping Concentration on $nTiO_2$ Structure

Powder XRD measurements were performed to examine the effect of doping and calcination on the crystal structure of $nTiO_2$. The as-synthesized (not calcined) samples did not exhibit any diffraction peaks, indicating the initial amorphous nature of the samples. Upon calcination, the samples were converted to crystalline oxides showing distinct Bragg peaks (Fig.1). XRD spectra of $Zr/nTiO_2$ calcined at 500 °C, with Zr concentrations of 0, 5, 10 and 15 mol% are shown in Fig. 1a. The peaks in the diffraction patterns correspond to the characteristic Bragg peaks of anatase TiO_2 (JCPDS card 00-021-1272). Only the XRD spectra for 10 and 15 mol % Zr (Fig.1a) show a slight hint for zirconia formation (barely visible peak at 30.55 º; JCPDS card 79-1771). The weakness of the peak is attributed to the relatively low zirconia concentration and the well dispersed Zr^{4+} ions within the crystalline $nTiO_2$ matrix. However, it is assumed that the concentration of a ZrO_2 phase will increase (and hence peaks at 35.40º, 50.70º and 60.35º in the pattern appear) if higher Zr doping concentrations are chosen. Finally, rather than having a mixed crystal system with a secondary phase segregated from $nTiO_2$, the diffusion of Zr into the $nTiO_2$'s crystal lattice results in one single phase; an outcome beneficial for uninterrupted electron transport during DSSC operation. Travelling electrons run a smaller risk of recombination, as they do not encounter any grain boundaries, which are common places for traps.

Fig. 1 also shows that Zr-doped samples exhibit a slight peak shift towards smaller angles (compare to pure $nTiO_2$ sample; Fig.1a, 0 mol % Zr, green), a fact confirming our

hypothesis that Zr^{4+} is well dispersed within the TiO_2 crystal lattice. The crystal structures of ZrO_2 and TiO_2 are very similar and Zr^{4+} ions can easily substitute for Ti^{4+} ions in the anatase matrix. However, the lattice structure of TiO_2 will be locally deformed close to a Zr exchanged in the crystal structure. The reason for this is the difference in ionic radii of Ti^{4+} and Zr^{4+} (Ti^{4+} = 61 pm, Zr^{4+} = 72 pm) [23,24]. It can therefore be concluded that Zr doping causes an expansion of the anatase lattice parameters with respect to the pure anatase phase at locations where Zr ions have replaced Ti, resulting in a slight shift of XRD peaks to smaller diffraction angles. This shift becomes more pronounced with increasing doping concentration, and is most noticeable at the 38.0°, 48.6°, and 63º diffraction peaks for the 15 mol % Zr sample (Fig.1 a, red).

In Figure 1b, the doping concentration of $Zr/nTiO_2$ samples is kept constant at 10 mol %, but the calcination temperature is increased from 400° C to 700º C. These results show that Zr doping suppresses the anatase-to-rutile phase transition [25]. No phase transformation from anatase to rutile was found across the 10 mol % Zr samples, although they were calcined at temperatures expected to cause an anatase-to-rutile phase transition [26]. Instead, the anatase crystal structure was maintained with relative peak intensities increasing with calcination temperature. This stabilization of the anatase phase can be explained by the fact that Zr^{4+} is more electropositive than Ti^{4+}. As such, the electronic cloud in $nTiO_2$, containing Zr doping, will be more loosely held, thus favouring the formation of the less dense anatase phase over the denser rutile phase [15]. In other words, the tight packing arrangements required for rutile phase formation is fully suppressed by the substitution of Ti^4 by Zr^{4+} in the crystal lattice. Furthermore, the larger size and higher electropositivity of Zr^{4+} compared to Ti^{4+} allows the lattice to exhibit better bonding

properties, and thus higher thermal stability than pure $nTiO_2$ [15,16]. The diffraction peaks in Fig. 1b maintain and even improve their sharpness with increasing calcination temperature, a hint of an increase in crystallinity and crystallite sizes assembling the NPs (Debye–Scherrer equation [16]), a result confirming also findings by Kim et al. [25].

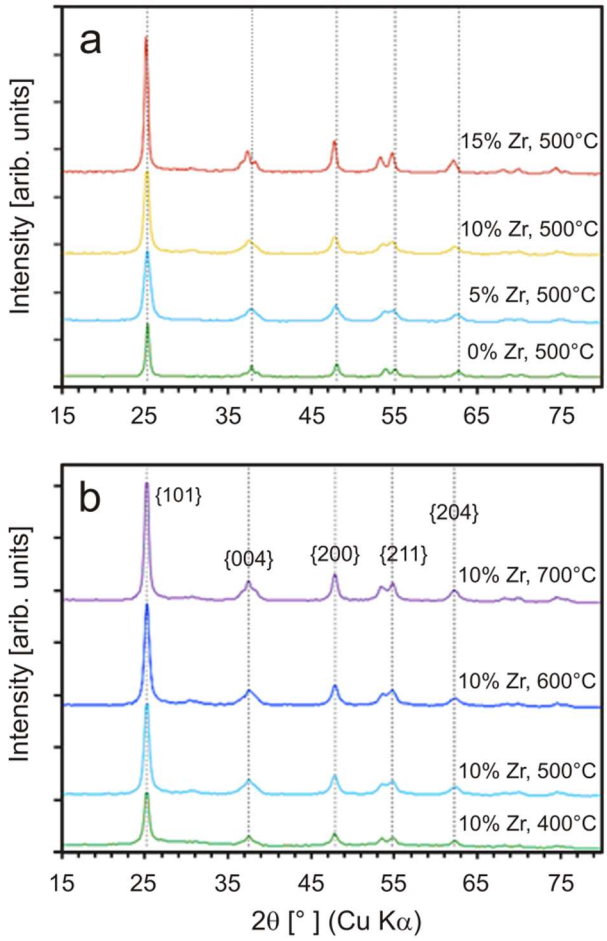

Figure 1. XRD spectra of $Zr/nTiO_2$: a) samples doped with 0, 5, 10 and 15% Zr and calcined at 500 ºC; b) samples doped with 10 mol % Zr and calcined at 400, 500, 600 and 700°C. Crystal structure identification and Miller indexing was carried out according to JCPDS card No. 21-1272 (TiO_2; anatase). Note: Doping of more than 10% Zr leads to a shift of the diffraction pattern as a result of unit cell expansion.

The effect of Zr-doping concentration on SSA and pore structure at various calcination temperatures was studied by N_2 physisorption and BET analysis. The adsorption-desorption isotherms of a selection of $nTiO_2$ and $Zr/nTiO_2$ samples are shown in Fig. 2, the corresponding SSA in Fig.3 and the average aggregate sizes of the samples are listed in Table 2. All samples demonstrated type IV adsorption isotherms [27] regardless of doping and thermal treatment, indicating that the samples are of porous nature [28]. In addition, all samples exhibit a single hysteresis and the hysteresis loops are all type H1 [29], indicating that the samples are porous NP-aggregates [30]. The locations of the hysteresis loops lay between 0.4 and 0.8 of the relative pressure (P/P^o) scale, which is an indication for mesoporous capillary condensation reaction [31]. Note: only the pure $nTiO_2$ (0 mol % Zr) samples demonstrated a clear decrease in N_2 sorption with increasing calcination temperature, indicating a decrease of the porous nature.

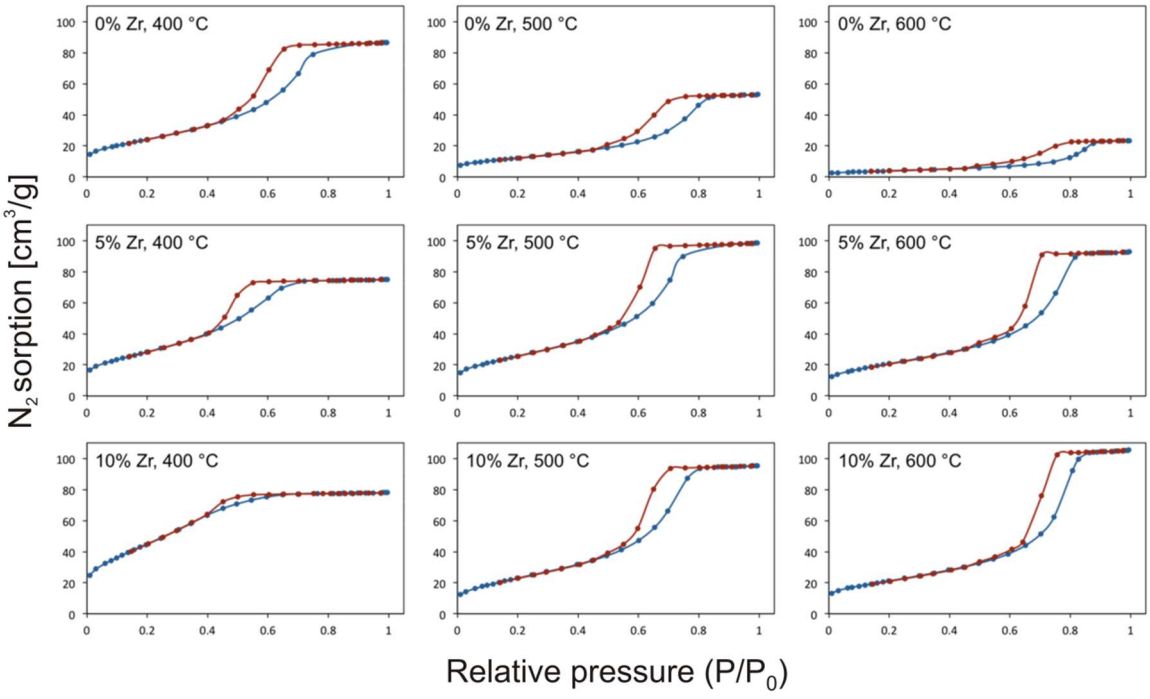

Figure 2. N_2 adsorption (blue) and desorption (red) isotherms of various Zr/nTiO_2 samples: from left to right increasing calcination temperature, from top to bottom increasing Zr concentrations. Isotherms of samples doped with 15 mol % Zr and samples calcined at 700º Care omitted as they show a similar behavior.

Crystallinity of the semiconductor is critical for efficient electron transport in a DSSC. Crystallinity is typically achieved at calcination temperatures of ~500 ºC. Also a large SSA is necessary to maximize the amount of dye molecules that can adsorb onto the porous semiconductor substrate allowing for maximal sunlight absorption. Unfortunately, these are competing effects, as some surface area is inevitably lost by porous semiconductor matrix collapsing during thermal treatment. The extent to which Zr doping moderates this tradeoff is obtained from the BET data of N_2 (Fig. 3 and Table 2).

Fig. 3 compares the SSAs of $nTiO_2$ and Zr/nTiO2 at various Zr concentrations and with respect to the calcination temperature. The highest SSA of 167 m^2/g was achieved with 10 mol % Zr doping at 400º C. The SSA decreased with increasing calcination temperature for all doping concentrations. The un-doped $nTiO_2$ sample (0 mol % Zr) lost nearly all of its SSA at 700º C. The doped samples calcined at 700º C however experienced considerably less structural collapse. The 5 mol % Zr sample retained nearly half of its original SSA. The pure $nTiO_2$ samples showed the lowest SSA within each measured temperature series. The SSA increased from pure TiO_2 to the 5 mol % Zr over all calcination temperature treatments. A further increase in Zr concentration led to an additional and strong increase of SSA for the 400° C sample (however, for the 15 mol % the SSA decreased), but a less pronounced gain for the 700° C sample. The two intermediate temperatures of 500° C and 600° C showed either a more stable (600° C) or a decreasing (500° C) SSA with increasing Zr concentration. There was no systematic behavior on the SSA with increasing Zr concentration beyond 5 mol %. In general, it was found that (Fig. 3 and Table 2): a) with increasing calcination temperature the average aggregate size increased, b) with increasing average aggregate size, the SSA decreased and c) the addition of Zr increased the SSA. This is in excellent agreement with Kim et al. [19] who found that Zr addition had a positive effect on the stabilization of pore structure.

The decrease in SSA with increasing aggregate size is in excellent agreement with the XRD data. The peaks sharpened, therefore the FWHM (full width half maximum) decreased with increasing calcination temperature. Taking the Debye -Scherrer equation [16] into account (where the crystallite size can be calculated from XRD peaks, with the FWHM located in the denominator), the size of the individually formed crystallites

increased with increasing calcination temperature, lowering the amount of voids forming the pores until complete collapse occurs at the highest examined calcination temperature.

It can therefore be concluded that the SSA decrease of $nTiO_2$ during the calcination process is considerably reduced when doped with Zr, demonstrating the thermo-stabilizing properties of the dopant. The 5 mol % Zr sample, showing the best results in surface area retention, also demonstrated the best aggregate size retention, exhibiting the best durability against thermal treatment.

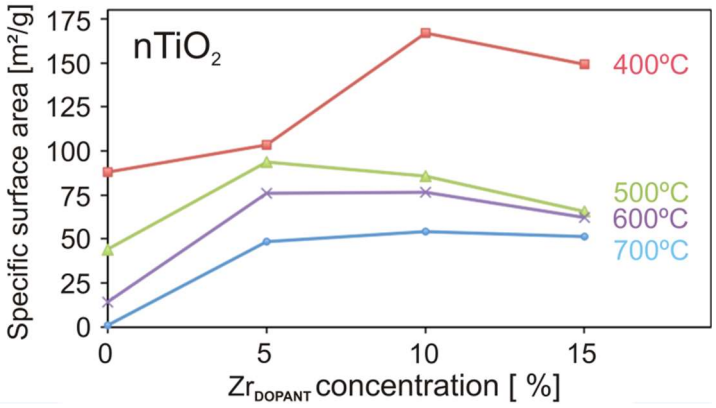

Figure 3. Specific surface areas of $nTiO_2$ samples doped with 0, 5, 10 and 15 mol % Zr and calcined at various temperatures.

Table 2: Average aggregate size from N_2 physisorption of $nTiO_2$ samples doped with 0-15 mol % Zr and calcined between 400°-700º C.

Average aggregate size (nm)				
T (°C)	0 mol % Zr	5 mol % Zr	10 mol % Zr	15 mol % Zr
400	68.3	58.0	36.0	40.3
500	135.8	63.9	69.9	91.1
600	420.5	79.3	78.6	96.4
700	5904.3	123.0	111.2	116.6

The morphology of the samples was investigated via SEM. The SEM micrographs (Fig. 4) depict NP aggregates confirming the porous nature of the $nTiO_2$ and $Zr/nTiO_2$ samples and show a spherical shape for the individual NPs for all examined Zr concentrations and calcination temperatures. As observed in Fig. 4, calcination T and time had little effect on the observed morphology, which is attributed to the stabilizing effect of Zr.

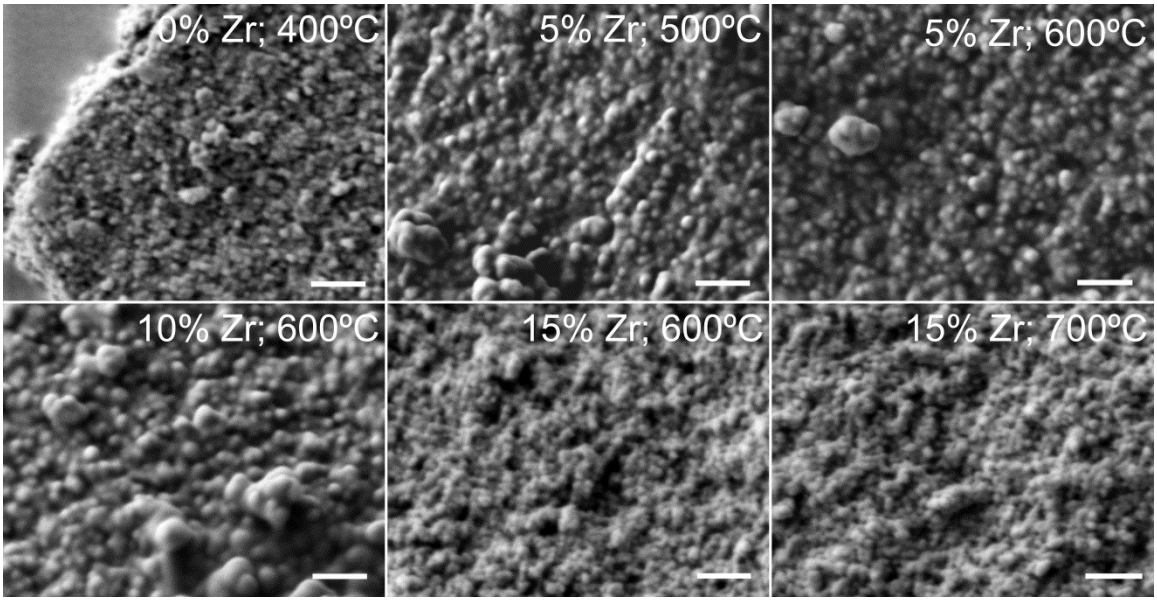

Figure 4. SEM images of a selection of Zr/nTiO_2 samples doped with increasing Zr concentrations (0 to 15 mol %) and calcined at various temperatures (400° - 700º C). The scale bars are 200 nm.

Energy dispersive X-ray spectrometer (EDS), a component of the SEM, was used to estimate the elemental composition of the samples, in particular the concentration of Zr (spectra not shown). The EDS-estimated Zr content of measured Zr/nTiO_2 samples corresponded well with the intended doping concentrations, suggesting that most of the precursor reacted fully during synthesis.

3.2 Performance of DSSCs using Zr/nTiO_2

Dye-sensitized solar cells (DSSCs) were fabricated using the experimental Zr/nTiO_2 NPs as the semiconducting layer of the cell. Cells were fabricated according to the procedure described in the supporting information (SI). For statistical purposes, 6 cells were fabricated for each Zr concentration; the average of their performance data were taken to ensure representative results. The cells were tested under simulated sunlight (AM 1.5),

and their J-V characteristics were evaluated. In total, 16 different photoactive layer compositions were tested: 4 different Zr concentrations, each calcined at 4 different temperatures. Fig. 5 compares the resulting cell efficiencies. In addition, a commercial $nTiO_2$ material (P25) was tested. Without doping (blue), cell efficiencies dropped with increasing calcination temperature as expected; higher calcination temperatures caused the porous semiconductor structure to collapse, reducing the surface area and thus the potential dye adsorption sites, decreasing the light absorption capability of the cell. Upon addition of Zr into the $nTiO_2$ matrix (red, green, purple), the behavior of efficiency decrease with increasing calcination temperature was no longer observed. Rather, the efficiencies became relatively constant at their respective doping levels, taking the error bars into account. These efficiencies correlate well with the SSAs (Fig.3). The highest efficiencies were achieved with 5 mol % Zr, surpassing all other cells of different doping concentration, except for pure $nTiO_2$ calcined at 400 ºC. This relates well with the data obtained from N_2 physisorption experiments, where 5 mol % Zr/$nTiO_2$ demonstrated the best resistance to thermal degradation, achieving the best retention of surface area, and average aggregate size (Fig.3 and Table 1).

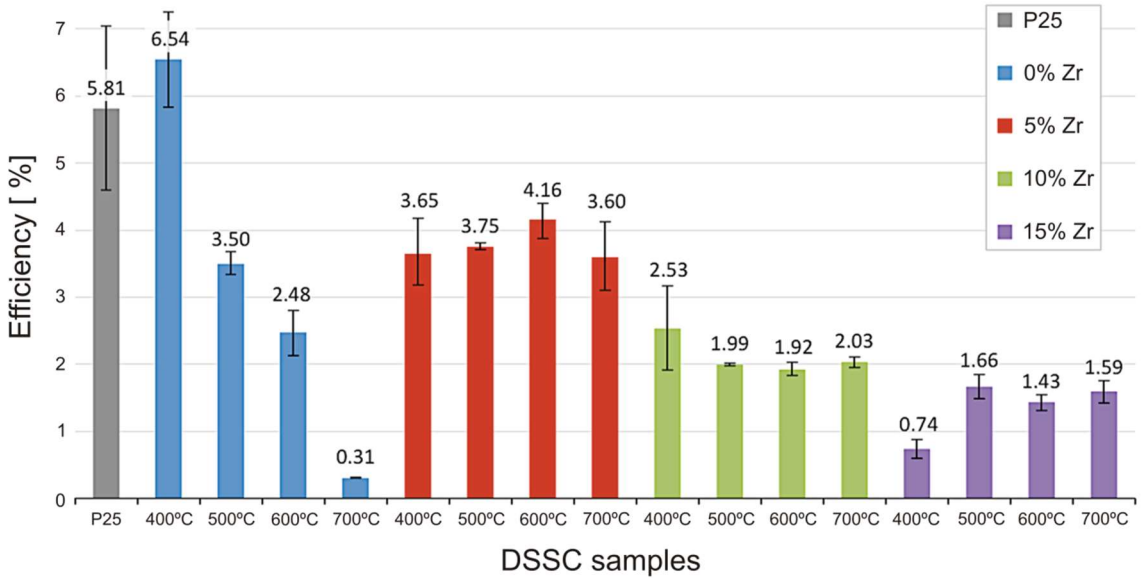

Figure 5. Energy conversion efficiency of DSSCs containing $nTiO_2$ and $Zr/nTiO_2$ as the semiconductor layer. Each value displayed represents an average of six cell efficiencies. For comparison: P25 (Degussa P25 Aeroxide, average particle size 21 nm, pure $nTiO_2$).

Zr has the best positive effect as a dopant in $nTiO_2$ for DSSCs when it is present at elevated calcination temperatures. This is relevant because many processing techniques require temperatures above 500º C. Based on our experimental results, if titania is processed at low temperatures, Zr doping is not necessary. Yet if elevated temperatures are used in emerging roll-to-roll fabrication with thermal or UV-curing where hot spots may occur, the addition of Zr will help prevent thermal degradation and improve the efficiencies.

The achieved efficiencies are comparable to DSSC characteristics found by Mohamed et al. [32] who investigated DSSC with electro-spun TiO_2 nanofibers being doped with 0.5, 1, 1.5 and 2 % zirconium and calcined at 500°C. They obtained efficiencies from 1.61 (without Zr doping) up to 4.51 for 1 % Zr. The Zr increase to 2 % decreased the efficiency to 2.31.

The photocurrent density-voltage (J-V) diagrams of the fabricated DSSCs are shown in Fig. 6. The corresponding photovoltaic characteristics derived from the J-V diagrams, such as open-circuit voltage (V_{OC}), short-circuit current density (J_{SC}), fill factor (FF) and energy conversion efficiency (η) [33] are listed in Table 3. At the lowest calcination temperature (400º C), pure $nTiO_2$ (blue) achieved the highest average efficiency of 6.54 % due to its high current density of 15.65 mA/cm^2. Without Zr however, the $nTiO_2$ structure collapsed when calcined at 700º C (Fig. 6d), diminishing viable surface area for dye adsorption sites, and reducing its current density to 1.08 mA/cm^2. An addition of 5 mol % Zr helped the $nTiO_2$ matrix preserve its structure at this high calcination temperature and maintain its surface area, evidence that Zr induces thermal stability. The increase in the SSA, as confirmed by the BET data (shown above), allowed for more electron pathways and increased the current density. The improved efficiency was indeed a result of enhanced photocurrent, as the V_{OC} remained relatively constant.

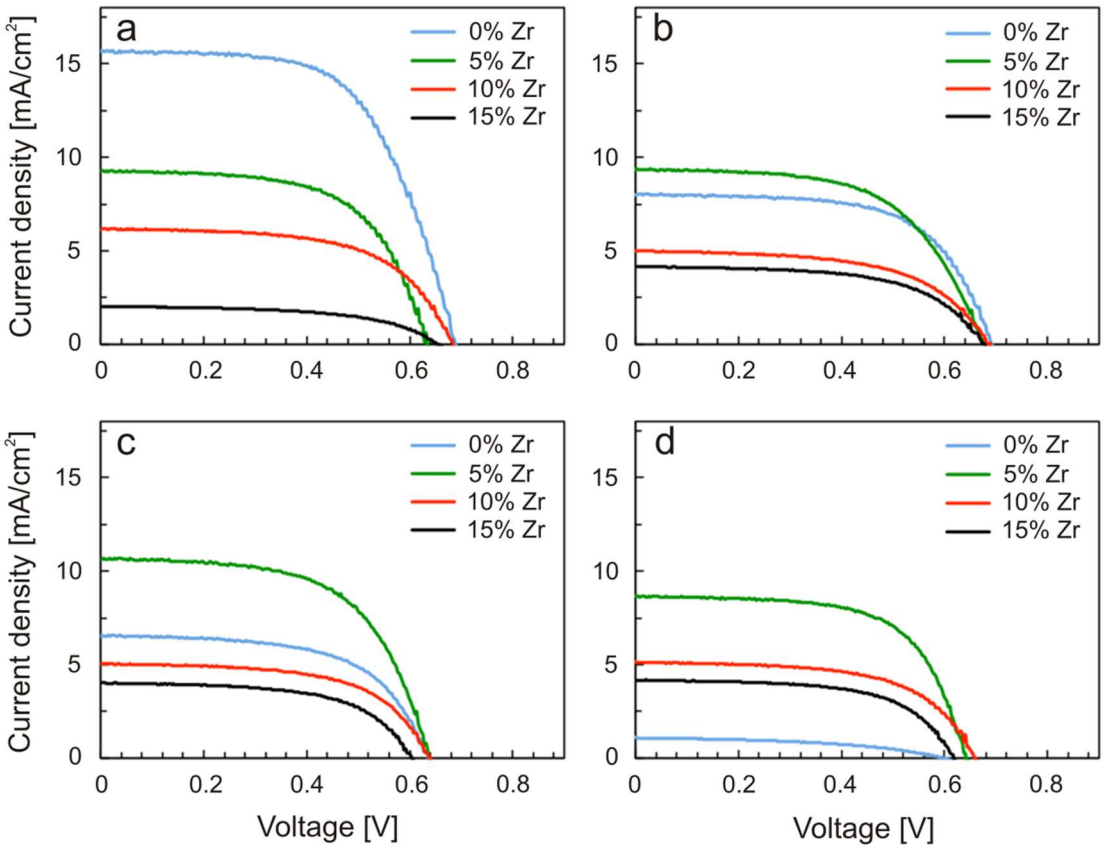

Figure 6. J-V diagrams for Zr-doped (0-15 mol %) nTiO_2-DSSCs, calcined at a) 400º C, b) 500º C, c) 600º C, and d) 700º C.

Table 3: J-V characteristics of DSSCs containing $nTiO_2$ and $Zr/nTiO_2$ at Zr concentrations from 5 - 15 mol % Zr.

Sample		V_{OC} (V)	J_{SC} (mA/cm^2)	FF	η (%)
400º	0 mol % Zr	0.69	15.65	0.61	6.54
	5 mol % Zr	0.63	9.26	0.62	3.65
	10 mol % Zr	0.68	6.17	0.60	2.53
	15 mol % Zr	0.65	2.02	0.55	0.74
500º	0 mol % Zr	0.69	8.01	0.63	3.50
	5 mol % Zr	0.67	9.34	0.60	3.75
	10 mol % Zr	0.69	4.99	0.58	1.99
	15 mol % Zr	0.68	4.16	0.59	1.66
600º	0 mol % Zr	0.63	6.55	0.60	2.48
	5 mol % Zr	0.64	10.66	0.61	4.16
	10 mol % Zr	0.64	5.04	0.60	1.92
	15 mol % Zr	0.60	4.01	0.59	1.43
700º	0 mol % Zr	0.63	1.08	0.45	0.31
	5 mol% Zr	0.65	8.65	0.64	3.60
	10 mol% Zr	0.66	5.12	0.60	2.03
	15 mol % Zr	0.62	4.19	0.62	1.59

15 mol % Zr-doped DSSCs (black) performed poorly at all calcination temperatures. ZrO_2 has a large band gap (~5.0 eV), and its reducing potential is more negative in its conduction band (CB) (and more-positive in its valence band) relative to those of TiO_2 [34]. This means that the lowest level of zirconia's CB is ~1.3 eV higher than titania's CB, and the higher doping level may be interfering negatively with the electronic transport processes of the semiconducting layer by enhancing the already-large band gap of TiO_2. If this is the case, the excited state of the dye molecules could be below the raised conduction band, and may thus be unable to inject electrons into the semiconductor's CB. The

electrons then transfer back to the dye, increasing the amount of recombination, explaining the observed lower current density in the 15 mol % Zr doped cells in comparison to their lesser doped counterparts. Future work will further examine the effect of lower Zr concentrations on DSSC efficiencies and their impact on charge transport properties.

3. Conclusions

In summary, this work represents a detailed study on the optimal Zr concentration needed for improved photovoltaic performance of dye-sensitized solar cells implementing Zr/nTiO_2. The addition of Zr into the photoactive layer of DSSCs has a distinct positive influence on the thermal stability of the semiconducting oxide's SSA and pore structure, and consequently device performance.

Zr/nTiO_2 samples at varying Zr concentrations and calcination temperatures were successfully synthesized using a modified sol-gel technique. XRD characterization confirmed that Zr ions were incorporated within the crystal structure of nTiO_2, which is beneficial for superior charge transport in DSSCs avoiding grain boundaries. High resolution TEM data in the future would be excellent to confirm the incorporation. The presence of Zr in the nTiO_2 matrix inhibited the anatase-rutile phase transition, and stabilized the lattice at high temperatures. The Zr/nTiO_2 had larger SSA than that of pure nTiO_2. The 5 mol % Zr samples demonstrated the best resistance to thermal degradation, achieving the best retention of surface area, and aggregate size.

Solar simulation studies demonstrated that DSSC performance was optimal at an intermediate doping concentration of 5 mol % Zr.

The dissipation of energy due to light absorption in a photovoltaic cell gives rise to several secondary effects, including local heat production, however zirconia can help preserve structure and increase stability at high temperatures. Although the highest cell efficiency was achieved with no Zr doping at 400 °C, the efficiencies of the no-doped cells dropped drastically with increasing calcination temperature, because the porous semiconductor matrix collapsed without the aid of a thermostabilizing agent. With the addition of zirconia embedded into the photoactive layer, this behavior was no longer observed, and except for pure titania at 400 °C, the 5% Zr samples demonstrated the best efficiencies, which was also reflected in their BET isotherm results. At each calcination temperature, higher surface area was achieved for samples containing zirconia rather than without zirconia.

Indeed, zirconia has a more advantageous effect as a dopant in TiO_2 when it is present at higher processing temperatures. This is relevant because many processing techniques in industry (not only in photovoltaics) require temperatures above 400 - 500 °C. If a material can be processed at low temperatures, then zirconia doping may not be necessary. However, when low temperature processing is not an option and elevated temperatures are needed, results show that adding Zr proves beneficial over the absence of Zr by inhibiting thermal degradation and improving the overall product performance.

Acknowledgement:

The authors would like to thank NSERC Strategic and Discovery programs for financial aid, the Western Nanofabrication Facility for help with electron microscopy. We also thank Lijuan Yang for her assistance with syntheses, XRD characterization and fruitful discussions as well as Qasem Alsharari for help with syntheses and Zakir Hossein for BET analysis.

References

[1] Shockley W and Queisser H J 1961 Detailed balance limit of efficiency of p-n junction solar cells *J. Appl. Phys.* **32** 510–519

[2] Kevin M, Fou Y H, Wong A S W and Ho G W 2010 A novel maskless approach towards aligned, density modulated and multi-junction ZnO nanowires for enhanced surface area and light trapping solar cells *Nanotechnology* **21** 315602

[3] Yong M J Q, Wong A S W and Ho G W 2009 Mesophase ordering and macroscopic morphology structuring of mesoporous TiO2 film *Mater. Chem. Phys.* **116** 563–568

[4] Agarwala S and Ho G W 2009 Synthesis and tuning of ordering and crystallinity of mesoporous titanium dioxide film *Mater. Lett.* **63** 1624–1627

[5] Dürr M, Rosselli S, Yasuda A and Nelles, G. 2006 Band-gap engineering of metal oxides for dye-sensitized solar cells *J. Phys. Chemistry* **110** 21899–902

[6] Kitiyanan A, Sakulkhaemaruethai S, Suzuki Y and Yoshikawa S 2006 Structural and photovoltaic properties of binary TiO_2-ZrO_2 oxides system prepared by sol-gel method *Compos. Sci. Technol.* **66** 1259–65

[7] Hernández-Alonso M D, Tejedor-Tejedor I, Coronado J M, Soria J and Anderson M A 2006 Sol-gel preparation of TiO_2-ZrO_2 thin films supported on glass rings: influence of phase composition on photocatalytic activity *Thin Solid Films* **502** 125–131

[8] Reidy D J, Holmes J D and Morris M A 2006 Preparation of a highly thermally stable titania anatase phase by addition of mixed zirconia and silica dopants *Ceram. Int.* **32** 235–39.

[9] Sui R and Charpentier P A 2012 Synthesis of metal oxide nanostructures by direct sol-gel chemistry in supercritical fluids *Chem. Rev.* **112** 3057–82

[10] Juma A, Acik I O, Oluwabi A T, Mere A, Mikli V, Danilson M and Krunks M 2016 Zirconium doped TiO_2 thin films deposited by chemical spray pyrolysis *Applied Surface Science* **387** 539-45

[11] Nemashkalo A B, Busko T O, Peters R M, Dmytrenko O P, Kulish M P, Vityuk N V, Tkach V M and Strzhemechny Y M 2016 Electronic band structure studies of anatase TiO_2 thin films modified with Ag, Au, or ZrO_2 nanophases *Phys. Status Solidi B* **253** 1754–64

[12] Lucky R A and Charpentier P A 2008 A one-step approach to the synthesis of ZrO_2-modified TiO_2 nanotubes in supercritical carbon dioxide *Adv. Mater.* **20** 1755–59

[13] Lucky R A, Medina-Gonzalez Y and Charpentier P A 2010 Zr doping on one-

dimensional titania nanomaterials synthesized in supercritical carbon dioxide *Langmuir* **26** 19014–21

[14] Sashchiuk A, Lifshitz E, Reisfeld R, Saraidarov T, Zelner M and Willenz A 2002 Optical and conductivity properties of PbS nanocrystals in amorphous zirconia sol-gel films *J. Sol-Gel Sci. Technol.* **24** 31–38

[15] Venkatachalam N, Palanichamy M, Arabindoo B and Murugesan V 2007 Enhanced photocatalytic degradation of 4-chlorophenol by Zr^{4+} doped nano TiO_2 *J. Mol. Catal. A Chem.* **266** 158–65

[16] Bendoni R, Mercadelli E, Sangiorgi N, Strini A, Sangiorgio A and Sanson A 2015 Alternative route for the preparation of Zr – doped TiO_2 layers for energy and environmental applications. *Ceram. Int.* **41** 9899–9909.

[17] Miao Z, Xu L, Song H, Zhao H and Chou L 2013 One-pot synthesis of ordered mesoporous zirconium oxophosphate with high thermostability and acidic properties *Catal. Sci. Technol.* **3** 1942-54.

[18] Namavar F, Wang G, Cheung C L, Sabirianov R F, Zeng X C, Mei W N, Bai J, Brewer J R, Haider H and Garvin K L 2007 Thermal stability of nanostructurally stabilized zirconium oxide. *Nanotechnology* **18** 415702

[19] Kim I, Song K-C, Wilhelm O and Pratsinis M E 2001 Sol-gel synthesis and spray granulation of porous titania powder *Chemie Ingenieur Technik* **73** 461-68

[20] Schattka J H, Shchukin D G, Jia J, Antonietti M and Caruso R A 2002 Photocatalytic activities of porous titania and titania/zirconia structures formed by using a polymer gel templating technique *Chem. Mater.* **14** 5103–08

[21] Linsebigler A L, Lu G and Yates J T 1995 Photocatalysis on TiO_2 surfaces: principles, mechanisms, and selected results *Chem. Rev.* **95** 735–58

[22] Chen Y, Zhou S, Gu G and Wu L 2006 Microstructure and properties of polyester-based polyurethane/titania hybrid films prepared by sol–gel process *Polymer* **47** 1640–48

[23] Abd El-Lateef H M and Khalaf M M 2015 Corrosion resistance of ZrO_2–TiO_2 nanocomposite multilayer thin films coated on carbon steel in hydrochloric acid solution *Mater. Charact.* **108** 29–41

[24] Zheleznov V V, Sushkov Y V, Voit E I, Sarin S A and Dmitrieva E E 2015 Effect of ZrO_2 on the structure of ZrO_2/TiO_2/SiO_2 nanocomposites fabricated by a template sol–gel method *J. Appl. Spectrosc.* **81** 983–89

[25] Kim J, Song K C, Foncillas S and Pratsinis S E 2001 Dopants for synthesis of stable

bimodally porous titania *J. Eur. Ceram. Soc.* **21** 2863–72

[26] Hanaor D A H and Sorrell C C 2011 Review of the anatase to rutile phase transformation *J. Mater. Sci.* **46** 855–74

[27] Keller J and Staudt R 2005 *Gas Adsorption Equilibria* (Boston, MA: Springer)

[28] Sing K S W 1985 Reporting physisorption data for gas/solid systems with special reference to the determination of surface area and porosity (Recommendations 1984). *Pure Appl. Chem.* **57** 603–19

[29] Sing K S W and Williams R T 2004 Physisorption hysteresis loops and the characterization of nanoporous materials *Adsorption, Science and Technology* **22** 773-82

[30] Allen T 1990 *Particle Size Measurements* (Netherlands: Springer)

[31] Lowell S, Shields J E and Morral J E 1985 *Powder surface area and porosity*, 2nd Edition (Springer)

[32] Mohamed I M A, Dao V-D, Barakat N A M, Yasin A S, Yousef A and Choi H-S 2016 Efficiency enhancement of dye-sensitized solar cells by use of ZrO_2-doped TiO_2 nanofibers photoanode *Journal of Colloid and Interface Science* **476** 9-19

[33] Mazer J A 1997 *Solar cells: an introduction to crystalline photovoltaic technology* (Boston, MA: Kluwer Academic Publishers)

[34] Chang S and Doong R 2006 Characterization of Zr-doped TiO_2 nanocrystals prepared by a nonhydrolytic sol - gel method at high temperatures **110** 20808–14